AGU PUBLICATIONS

Geophysical Research Letters

RESEARCH LETTER
10.1002/2015GL065903

**Key Points:**
- We track concentric GWs from their convective source region in the troposphere to the ionosphere
- Gravity wave features are seen nearly simultaneously in stratosphere, mesosphere, and ionosphere
- The slant propagation path of the TIDs suggests their source being near the convective storm

**Correspondence to:**
I. Azeem,
iazeem@astraspace.net

**Citation:**
Azeem, I., J. Yue, L. Hoffmann, S. D. Miller, W. C. Straka III, and G. Crowley (2015), Multisensor profiling of a concentric gravity wave event propagating from the troposphere to the ionosphere, *Geophys. Res. Lett.*, *42*, 7874–7880, doi:10.1002/2015GL065903.

Received 24 AUG 2015
Accepted 21 SEP 2015
Accepted article online 25 SEP 2015
Published online 14 OCT 2015



# Multisensor profiling of a concentric gravity wave event propagating from the troposphere to the ionosphere

**Irfan Azeem[1], Jia Yue[2], Lars Hoffmann[3], Steven D. Miller[4], William C. Straka III[5], and Geoff Crowley[1]**

[1]ASTRA LLC, Boulder, Colorado, USA, [2]Atmospheric and Planetary Sciences, Hampton University, Hampton, Virginia, USA, [3]Forschungszentrum Jülich, Jülich, Germany, [4]Cooperative Institute for Research in the Atmosphere, Colorado State University, Fort Collins, Colorado, USA, [5]Cooperative Institute for Meteorological Satellite Studies, University of Wisconsin Madison, Madison, Wisconsin, USA

**Abstract** In this paper, we present near-simultaneous observations of a gravity wave (GW) event in the stratosphere, mesosphere, and ionosphere over the South Central United States and track it from its convective source region in the troposphere to the ionosphere, where it appears as a traveling ionospheric disturbance (TID). On 4 April 2014 concentric GW ring patterns were seen at stratospheric heights in close proximity to a convective storm over North Texas in the Atmospheric Infrared Sounder data on board the NASA Aqua satellite. Concentric GWs of similar orientation and epicenter were also observed in mesospheric nightglow measurements of the Day/Night Band of the Visible/Infrared Imaging Radiometer Suite on the Suomi National Polar-orbiting Partnership satellite. Concentric TIDs were seen in total electron content data derived from ground-based GPS receivers distributed throughout the U.S. These new multisensor observations of TIDs and atmospheric GWs can provide a unique perspective on ionosphere-atmosphere coupling.

## 1. Introduction

Atmospheric gravity waves (GW) are an important driver of the upper atmospheric circulation. In particular, they are responsible for the high-latitude cold summer mesopause (~90 km altitude), which is constantly bathed in sunlight, yet being about 100 K colder than the high-latitude winter mesopause, which is in complete darkness [*Holton*, 1982]. Furthermore, GWs with periods of less than about 1 h are responsible for much of the wave-induced transport (and incipient forcing) that occurs in the mesosphere/lower thermosphere region [*Fritts and Vincent*, 1987].

Mesospheric signatures of GW excited by processes occurring in the troposphere have been routinely observed in airglow measurements [*Taylor et al.*, 1995; *Takahashi et al.*, 1999; *Smith et al.*, 2000]. Theoretical understanding of upward GW propagation in the atmosphere suggests that while small spatial-scale GWs are confined to below the stratopause, the medium- and large-scale GWs have appropriate characteristic amplitudes and phase velocity to allow them to penetrate into the mesopause and beyond. Figure 4 from *Vadas* [2007] suggests that GWs with periods in the 10–80 min range and horizontal wavelengths between 100 and 1200 km can penetrate the bottomside *F* region ionosphere from their source in the troposphere.

One of the major sources of GWs is deep convection associated with strong thunderstorms [*Alexander and Pfister*, 1995]. Multiple studies have suggested that convective storms are likely to be the most important single-point source for GWs reaching the mesopause region and altering its mean state [*Alexander*, 1996]. Numerical simulations of convectively generated GWs have provided unprecedented details of their morphology and propagation characteristics [*Horinouchi et al.*, 2002; *Lane and Sharman*, 2006]. These studies indicate that these convectively generated GWs have conically shaped phase surfaces when propagating through a medium with small or zero background winds. When viewed in a two-dimensional plane, such as from a nadir-viewing airglow imager, these convectively generated GW appear as circular rings traveling outward away from the center of the cone [*Yue et al.*, 2009, 2014, *Miller et al.*, 2012]. Background winds have a directional filtering effect on propagation of gravity waves, causing them to appear as partial circular rings [*Yue et al.*, 2009].

Circular wave fronts have been also observed in GW propagating through the ionosphere (90–400 km). For example, concentric wave features in the ionosphere associated with a GW event, possibly generated by a tornadic thunderstorm, were first reported by *Nishioka et al.* [2013] in Global Position System (GPS) total

electron content (TEC) data from North America. While that study presented details of the horizontal morphology of a traveling ionospheric disturbance (TID) event associated with a tropospheric phenomenon, it did not provide any direct evidence of stratospheric and mesospheric GW propagation due to lack of available data. TIDs are signatures of GW motion at ionospheric heights. The motion of the neutral gas by GW sets the ionosphere into motion via collisional interactions. The resulting plasma motion displaces the isoionic contours, which when viewed at a fixed altitude appears as quasiperiodic fluctuation in plasma density.

Despite the frequent occurrence and long-lived nature of midlatitude TIDs, no observational studies have tracked GWs from their source regions in the lower atmosphere, through the middle atmosphere, and ultimately to the ionosphere. Being able to track GWs from their source region to the upper atmosphere regions where they dissipate is critical for advancing our understanding of the full chain of coupled plasma processes in the ionosphere-atmosphere system. Multisensor measurements of GWs at different heights can provide important information on wave coupling, propagation, and temporal variability of the atmosphere in response to local sources and filtering conditions. In this paper, we use multiple instruments on various satellites to show direct evidence of near-simultaneous observations of concentric GW in the stratosphere, mesosphere, and ionosphere over the South Central U.S.

This paper is organized as follows: Section 2 briefly describes the satellite and ground-based GPS TEC data used in this study. Section 3 presents satellite observations of the concentric GW event on 4 April 2014 over southeastern United States and the analysis of GW driven TIDs in GPS TEC data. Section 5 summarizes the key findings of this study and provides a discussion of these findings.

## 2. Data Sets

### 2.1. Atmospheric Infrared Sounder

The Atmospheric Infrared Sounder (AIRS) [*Aumann et al*., 2003] is a hyperspectral infrared spectrometer onboard the NASA Aqua satellite, launched in 2002. It contains 2378 channels taking measurements at 3.74–4.61 μm, 6.20–8.22 μm, and 8.8–15.4 μm wave bands. AIRS makes a cross-track scan every 2.67 s that includes 90 footprints on the ground. The outermost scan angle is ±48.95° from nadir, which provides a ~1800 km wide swath given Aqua's 705 km orbital altitude. The pixel footprint size increases from $14 \times 14\ km^2$ at the nadir to $42 \times 21\ km^2$ at the side, yielding an average cross-track footprint width of about 20 km. Previous GW studies using AIRS 15 μm and 4.3 μm $CO_2$ channel radiance variances with weighting function peaking at different levels in the stratosphere show strong correlations between the enhancement of GW amplitudes and deep convective activities in the summer hemisphere, in the tropics, and at midlatitudes [*Hoffmann and Alexander*, 2010; *Hoffmann et al*., 2013]. In this paper, we used the AIRS instrument's 4.3 μm $CO_2$ channel radiances (an atmospherically opaque band having peak sensitivity in the midstratosphere—at about 30–40 km above mean sea level) to detect gravity waves in the stratosphere. In addition, we used AIRS radiances at 8.1 μm [*Aumann et al*., 2006; *Hoffmann and Alexander*, 2010] to detect high clouds associated with deep convection, as this channel is fairly transparent (atmospheric window) through the troposphere and stratosphere.

### 2.2. Visible/Infrared Imaging Radiometer Suite

The Day/Night Band (DNB) sensor onboard the Suomi National Polar-orbiting Partnership (S-NPP) satellite, launched in 2011 as part of the Visible/Infrared Imaging Radiometer Suite (VIIRS), provides satellite-based sensing of the nocturnal environment [*Lee et al*., 2006; *Miller et al*., 2013a, 2013b]. It offers unprecedented spatial resolution of 0.742 km, with nearly fixed pixel size across a 3000 km swath. During initial calibration exercises, it became apparent that unanticipated low-light signals were present in DNB observations collected during New Moon. *Miller et al*. [2012] determined that the primary source of illumination was atmospheric nightglow emission, predominately from excited hydroxyl (OH*), molecular oxygen ($O_2$), and atomic oxygen (O). Signal magnitudes range from $10^{-11}$ to $10^{-9}\ W\ cm^{-2}\ sr^{-1}$ or roughly 100 times fainter than moonlight (which in turn is ~$10^5$ to $10^6$ times fainter than daytime scenes) and are observable by the S-NPP in its Sun-synchronous orbit during the ~2 week period surrounding the New Moon. Thus, the nightglow signal resides at the extreme lower bounds of DNB sensitivity, just above the instrument's noise floor, and is indiscernible in most moonlit scenes. *Miller et al*. [2012] further show that in addition to the reflected nightglow that enables low cloud and snow/ice detection, the DNB detects regions of direct (upwelling) nightglow emission

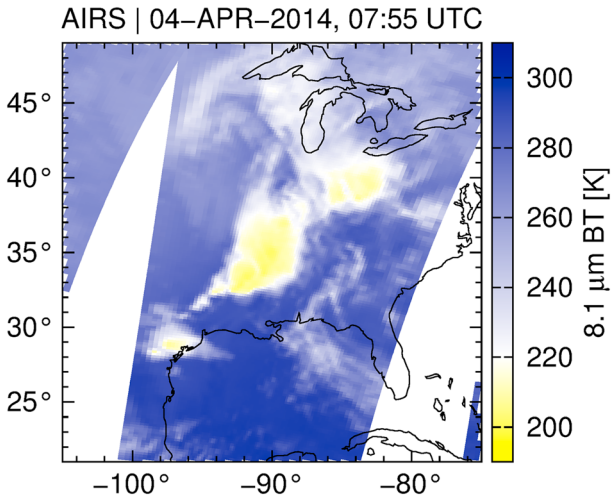


**Figure 1.** AIRS observations of clouds in the 8.1 μm channel showing convective storm over Texas on 4 April 2014 at 7:55 UTC.

from the principal nightglow emission layer (~85–90 km, near the mesopause). These direct emissions often reveal broad synoptic-scale (scale ~1000 km) patterns of nightglow variability and mesoscale structures caused by (scale ~10–100 km) GWs propagating through the free atmosphere or traveling along ducting layers.

### 2.3. GPS TEC

For this study we used GPS TEC data from over 4000 sites to image concentric TIDs observed over the contiguous United States (CONUS). Our approach was to process the GPS data and derive vertical TEC maps in a way similar to that presented by *Tsugawa et al.* [2011] and *Nishioka et al.* [2013]. In brief, we used the pseudo-range and phase measurements of GPS signals at L1(1575.42 MHz) and L2 (1227.6 MHz) frequencies to derive slantwise TEC information, which was then converted to vertical TEC (VTEC) using the obliquity factor model described by *Kaplan and Hagerty* [2006]. In mapping slantwise TEC to VTEC, we used the International Reference Ionosphere (IRI) model to determine the ionospheric pierce point (IPP) altitude to be 350 km. We then computed perturbations in TEC by detrending VTEC using a 20 min running mean for each GPS satellite followed by 0.15° × 0.15° binning in latitude and longitude and then horizontally smoothing the resulting TEC map using a two-dimensional (2-D) Gaussian filter, as described by *Nishioka et al.* [2013].

## 3. Results and Discussions

We have brought together the AIRS, DNB, and TEC observations to provide an unprecedented cross-sectional view of GW propagating upward through the atmosphere. Figure 1 shows AIRS cloud imagery in 8.1 μm brightness temperature (BT) data over the CONUS on 4 April 2014, at about 07:55 UTC. The figure shows a deep convective system extending from Texas northeastward to the Ohio River Valley. Around the same time, the National Weather Service Storm Prediction Center reported severe storm activity in the South Central U.S., including several tornados in North Texas. The AIRS brightness temperature minimum above the Texas storms was close to 200 K, well below climatological zonal-mean tropopause temperatures of 210 to 215 K [*Hoffmann et al.*, 2013], implying deep convection overshooting the tropopause in this region.

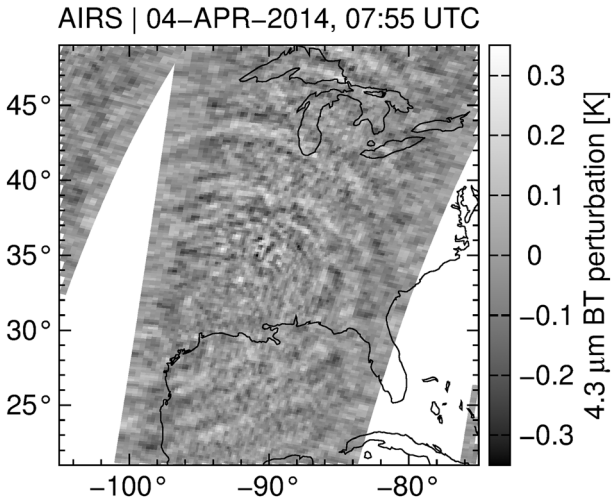


**Figure 2.** AIRS-derived 4.3 μm brightness temperature perturbations showing concentric GW emanating from the deep convection region above Mississippi on 4 April 2014 at 7:55 UTC.

Figure 2 shows the AIRS 4.3 μm BT perturbation map over the CONUS. BT perturbations have been calculated by subtracting a fourth-order polynomial fit for each across-track scan from the individual BT measurements for each satellite footprint. This detrending procedure removes background signals related to large-scale temperature gradients and planetary waves [*Hoffmann et al.*, 2013]. The figure shows concentric GW in the stratosphere emanating from

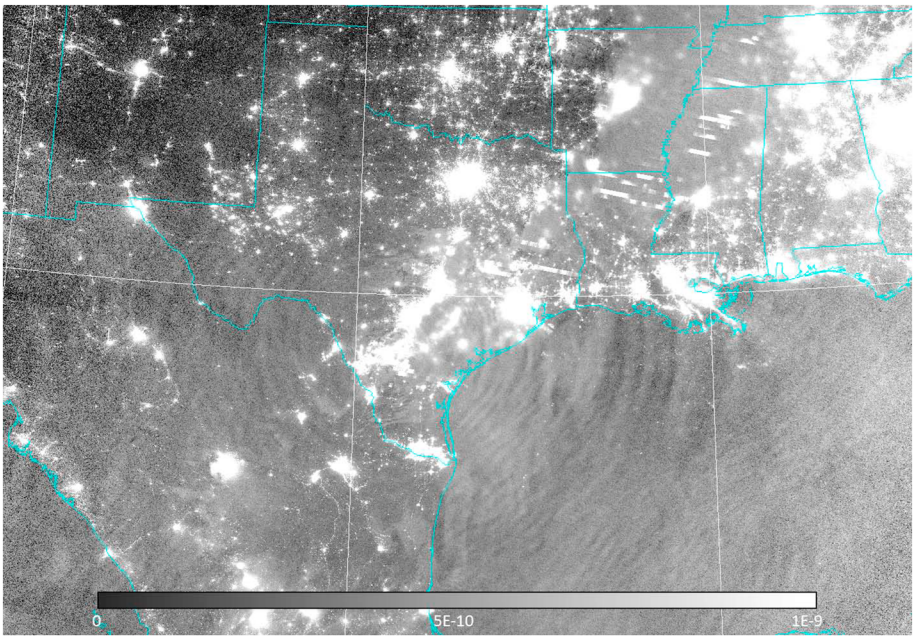


**Figure 3.** Concentric gravity wave image in VIIRS/DNB measurements on 4 April 2014 at 8:08:59 UTC.

the convective storm. Due to the coverage gap between adjacent AIRS swaths we were not able to create a full composite image showing complete radial patterns of the GW event. However, the concentric wave features thought to be associated with the convective activity are readily discernable through visual inspection. Their horizontal wavelength is approximately 250 km. The AIRS data also reveal small-scale waves to the southwest of the larger-scale waves, with horizontal wavelength on the order of 40 km.

Moving upward to the mesopause and the nightglow layer near 85–90 km, Figure 3 shows concentric GW centered over Texas in the S-NPP VIIRS/DNB band measurements on 4 April 2014 at 8:08:59 UTC (within 15 min of the Aqua/AIRS overpass crossing the convective line). The horizontal resolution of VIIRS/DNB is much higher than that of AIRS, explaining the finer structures visible in DNB measurements (~30–40 km horizontal wavelength). Light sources from urban areas also appear in the figure as bright white pixels. There are a number of lightning stripes located over the high clouds. Note that there are also larger-scale wave features of 200–300 km in the Gulf of Mexico.

Figure 4 shows a sequence of TEC data mapped over the CONUS on 4 April 2014 at 7:40, 9:10, 9:50, and 10:30 UTC. We should point out here that the gray scale in the figure represents the weighed sum of the perturbations over the specified latitude/longitude grid, which is significantly lower than the actual TID amplitude; the gray scale ranges should not be confused with the magnitude of the TEC perturbation. The unsmoothed amplitude of the TIDs as seen in the TEC time series of an individual GPS receiver is about ±0.1 TECU (~1% of the background TEC) with an uncertainty of 0.02 TECU. The TEC map at 8:30 UTC (Figure 4a) does not show any coherent wave structure. At 9:10 UTC (Figure 4b), two sets of circular wave fronts can be seen in the figure, one extending from Texas to Ohio. The center of these TIDs is located over Texas in the vicinity of the connective storm regions (shown in Figure 1). The storm-generated concentric TIDs are also present in the TEC map at 9:50 UTC. A full TEC map sequence (not shown here) at a cadence of 30 s shows that the TIDs propagate radially outward from the center and they are visible in GPS TEC data for about 70 min. By 10:30 UTC, the concentric TIDs had largely dissipated in the TEC map over the CONUS.

A wavelet spectrogram of the GPS TEC data yielded various TID perturbation parameters. Based on the wavelet analyses we estimated the TID period to be 20.8 ± 2.1 min, its horizontal wavelength to be 251.5 ± 6.2 km, and the horizontal phase speed to be 201.3 ± 15.5 m/s. The wavelength of the TID is consistent with that of the stratospheric GWs observed in AIRS data. The small-scale GWs seen in the AIRS and DNB data cannot be detected in GPS data because of its coarser resolution (15 km) and spatial smoothing.

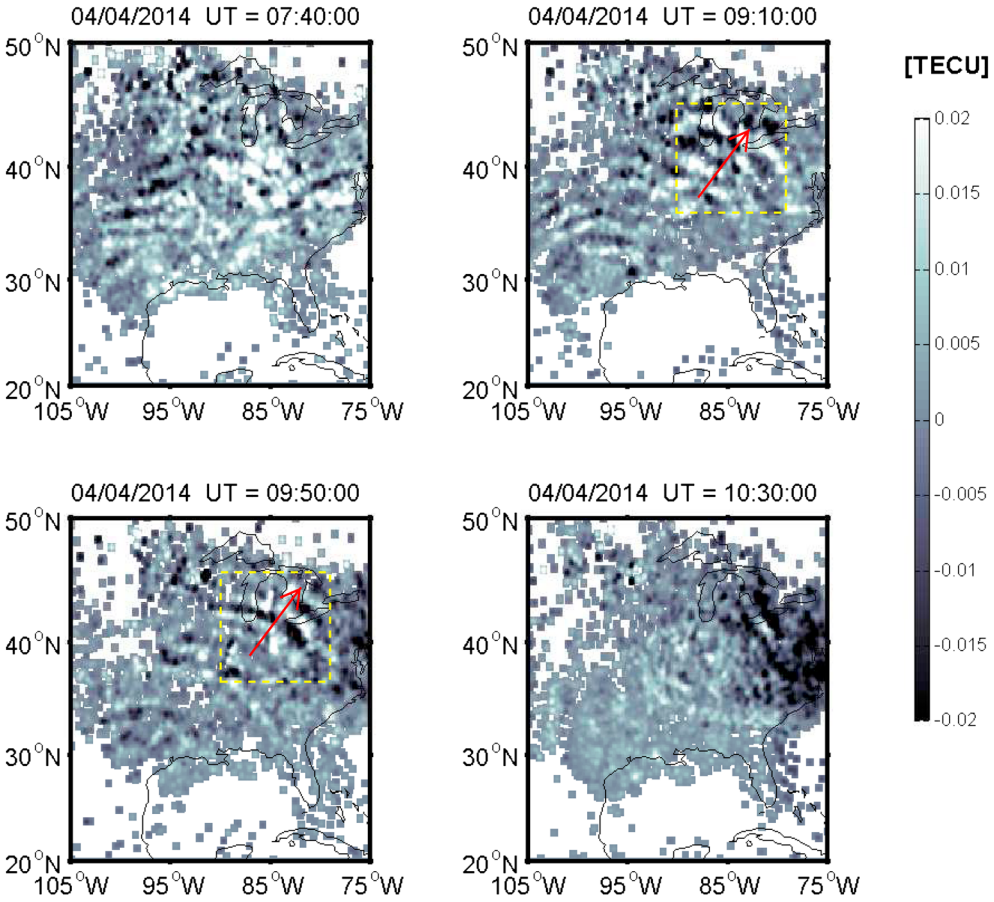


**Figure 4.** TEC perturbation maps showing concentric wavefronts over the CONUS derived from about 4000 GPS sites on 4 April 2014 at (a) 08:30 UTC, (b) 09:10 UTC, (c) 09:50 UTC, and (d) 10:30 UTC. The color scale is ±0.02 TECU (1 TECU = $1 \times 10^{16}$ el/m$^2$).

## 4. Discussions and Summary

In this paper we have used multiinstrument data sets offering sensitivity to different levels of the upper atmosphere to track concentric GWs from their convective source region in the troposphere over North Texas on 4 April 2014 to the ionosphere where they appeared as TIDs. Intense areas of convection are known to produce a broad spectrum of GWs, a subset of which survive breaking and absorption in the stratosphere and mesosphere to reach the mesopause and above. The composite measurements clearly illustrate this transfer process.

In a convective region, instantaneous forcing of the overshooting plume can generate a broad spectrum of GWs. Due to their dispersive nature, the GWs launched by the storms spread out in space and time as they propagate vertically, leading to conically shaped phase surfaces [see *Yue et al*., 2013, Figure 1]. The horizontal spreading of a GW is a function of waves period, horizontal wavelength, and speed. The AIRS data show a convective storm system over the southeastern U.S. and concentric gravity waves emanating from these convective regions. A close examination of the AIRS 4.3 μm radiance data show two groups of concentric GWs; one likely to be generated by the storm to the southwest and the other associated with the larger storm shown in Figure 1. Along with the larger-scale GWs (~250 km horizontal wavelength), the AIRS 4.3 μm data also reveal many small-scale waves with horizontal wavelength on the order of 40 km. However, dissipation properties of GWs for a typical temperature profile of the atmosphere for the date and time shown here suggest that these small-scale waves will tend to dissipate much lower in the atmosphere and will not able to penetrate the ionosphere [*Vadas*, 2007]. This could explain why the GPC TEC data only shows TIDs with a horizontal wavelength of ~250 km. Furthermore, the effect of Gaussian smoothing of TEC data in latitude and longitude could also contribute to this by averaging out smaller-scale waves.

To test our hypothesis that the observed TIDs were likely excited by the convective storms over Texas seen in the AIRS data (Figure 1), we computed the oblique propagation path of the GW and compared the base of the ray path to the storm locations. As noted before, the dispersion relation suggests that different GW periods propagate at different angles to the horizontal [*Fritts and Alexander*, 2003]. Using a simplified formulation presented by *Vadas and Nicolls* [2009] (which neglects background horizontal winds), we can write the propagation angle as follows:

$$\sin\theta = \left({}^{\tau_B}/_{\tau_r}\right) \tag{1}$$

where $\theta$ is the angle between the horizontal and the direction of propagation of the atmospheric GW (AGW), $\tau_r$ is the TID period, and $\tau_B$ is the buoyancy period. Using the buoyancy period of $\tau_B$ ~10.4 min (calculated using the Mass Spectrometer and Incoherent Scatter Radar model at 350 km), we find that $\theta \sim 30°$ for the AGWs with $\tau_\rho \sim 21$ min from equation (1). Assuming that the IPP is at 350 km, we estimate the horizontal distance traveled by the GW to be ~614 km.

This horizontal puts the source location of the TIDs in the general vicinity of the convective storms imaged in AIRS data (see Figure 1). These results suggest that the TIDs observed in TEC data could indeed have been driven by GWs generated by the convective storms over Texas seen in AIRS data.

The key findings of this study are summarized below:

1. The deep penetration of GWs from the troposphere to the ionosphere is observed and reported for the first time using multiple data sets. The GW event shown in this study occurred in April, an equinox month, when the background wind is weak [*Yue et al*., 2009]. This confirms the suggestion by *Yue et al*. [2009] that equinox seasons might be ideal for observing concentric gravity waves in the upper atmosphere.
2. Although the propagation of small-scale GWs is symmetric in DNB, the larger-scale GWs of ~250 km wavelength predominantly were propagating eastward, even in the stratosphere. This probably could be the result of wind filtering, which will be further explored in future studies.
3. The GW images in AIRS, DNB, and TEC data may not show exactly the same GWs because the time offset between different observations may not match the exact propagation time from the stratosphere to the mesopause or from the mesopause to the ionosphere. However, the morphology and horizontal scales of the observed GWs suggest that they were likely excited by the same storm system.

This work provides the first concrete evidence that the TIDs observed in TEC data were forced by the gravity waves excited by thunderstorms over southeastern U.S. The results presented here provide information regarding the transportation of wave energy and momentum over large distances, and the morphological characteristics of TIDs. The TID images in GPS TEC data can also shed new light on the directional filtering of GWs by atmospheric winds that will permit gravity wave packets propagating against the winds to reach the ionosphere with minimum energy loss. For the first time, we provide multilayer constraint for gravity wave resolving models such as the high-resolution Whole Atmosphere Community Climate Model [*Liu et al*., 2014], which extends from the ground to the upper atmosphere. This is important for modern general circulation model development.

**Acknowledgments**
This work was partially supported by the NASA contract NNH13CJ33C and the ONR award FA9550-07-1-0565 to ASTRA. We acknowledge the use of publicly available ground-based GPS TEC data from the Southern California Integrated GPS Network, International GPS Service for Geodynamics, UNAVCO, Hartebeesthoek Radio Astronomy Observatory, Natural Resources Canada, Geoscience Australia, the Brazilian Institute of Geography and Statistics, University of New Brunswick, National Oceanic and Atmospheric Administration, and National Aeronautics and Space Administration.

## References

Alexander, M. J. (1996), A simulated spectrum of convectively generated gravity waves: Propagation from the tropopause to the mesopause and effects on the middle atmosphere, *J. Geophys. Res.*, *101*, 1571–1588, doi:10.1029/95JD02046.

Alexander, M. J., and L. Pfister (1995), Gravity wave momentum flux in the lower stratosphere over convection, *Geophys. Res. Lett.*, *22*, doi:10.1029/95GL01984.

Aumann, H. H., D. Gregorich, and S. M. DeSouza-Machado (2006), AIRS observations of deep convective clouds, *Proc. SPIE*, *6301*, 63010J, doi:10.1117/12.681201.

Aumann, H. H., et al. (2003), AIRS/AMSU/HSB on the Aqua mission: Design, science objectives, data products, and processing systems, *Geosci. Remote Sens. IEEE Trans.*, *41*(2), 253–264.

Fritts, D. C., and M. J. Alexander (2003), Gravity wave dynamics and effects in the middle atmosphere, *Rev. Geophys.*, *41*, 1003, doi:10.1029/2001RG000106.

Fritts, D. C., and R. A. Vincent (1987), Mesospheric momentum flux studies at Adelaide, Australia: Observations and a gravity wave-tidal interaction model, *J. Atmos. Sci.*, *44*, 605.

Hoffmann, L., X. Xue, and M. J. Alexander (2013), A global view of stratospheric gravity wave hotspots located with Atmospheric Infrared Sounder observations, *J. Geophys. Res. Atmos.*, *118*, 416–434, doi:10.1029/2012JD018658.

Hoffmann, L., and M. J. Alexander (2010), Occurrence frequency of convective gravity waves during the North American thunderstorm season, *J. Geophys. Res.*, *115*, D20111, doi:10.1029/2010JD014401.

Holton, J. R. (1982), The role of gravity wave induced drag and diffusion in the momentum budget of the mesosphere, *J. Atmos. Sci.*, *39*, 791.

Horinouchi, T., T. Nakamura, and J.-I. Kosaka (2002), Convectively generated mesoscale gravity waves simulated throughout the middle atmosphere, *Geophys. Res. Lett.*, *29*(21), 2007, doi:10.1029/2002GL016069.

Kaplan, E. D., and C. Hagerty (2006), *Understanding GPS: Principles and Applications*, 2nd ed., Artech House, Norwood, Mass.

Lane, T. P., and R. D. Sharman (2006), Gravity wave breaking, secondary wave generation, and mixing above deep convection in a three-dimensional cloud model, *Geophys. Res. Lett.*, *33*, L23813, doi:10.1029/2006GL027988.

Lee, T. F., S. D. Miller, F. J. Turk, C. Schueler, R. Julian, S. Deyo, P. Dills, and S. Wang (2006), The NPOESS/VIIRS day/night visible sensor, *Bull. Am. Meteorol. Soc.*, *87*(2), 191–199, doi:10.1175/BAMS-87-2-191.

Liu, H., J. M. McInerney, S. Santos, P. H. Lauritzen, M. A. Taylor, and N. Pedatella (2014), Gravity waves simulated by high-resolution Whole Atmosphere Community Climate Model, *Geophys. Res. Lett.*, *41*, 9106–9112, doi:10.1002/2014GL062468.

Miller, S. D., S. P. Mills, C. D. Elvidge, D. T. Lindsey, T. F. Lee, and J. D. Hawkins (2012), Suomi satellite brings to light a unique frontier of nighttime environmental sensing capabilities, *Proc. Natl. Acad. Sci. U.S.A.*, *109*, 39, doi:10.1073/pnas.1207034109.

Miller, S. D., W. Straka III, S. P. Mills, C. D. Elvidge, T. F. Lee, J. Solbrig, A. Walther, A. K. Heidinger, and S. C. Weiss (2013a), Illuminating the capabilities of the Suomi NPP VIIRS day/night band, *Remote Sens.*, *5*, 6717–6766, doi:10.3390/rs5126717.

Miller, S. D., W. Straka III, S. P. Mills, C. D. Elvidge, T. F. Lee, J. Solbrig, A. Walther, A. K. Heidinger, and S. C. Weiss (2013b), Illuminating the capabilities of the Suomi NPP VIIRS day/night band, *Remote Sens.*, *5*, 6717–6766, doi:10.3390/rs5126717.

Nishioka, M., T. Tsugawa, M. Kubota, and M. Ishii (2013), Concentric waves and short-period oscillations observed in the ionosphere after the 2013 Moore EF5 tornado, *Geophys. Res. Lett.*, *40*, 5581–5586, doi:10.1002/2013GL057963.

Smith, S. M., M. Mendillo, J. Baumgardner, and R. R. Clark (2000), Mesospheric gravity wave imaging at a subauroral site: First results from Millstone Hill, *J. Geophys. Res.*, *105*, 27,119–27,130, doi:10.1029/1999JA000343.

Takahashi, H., P. P. Batista, R. A. Buriti, D. Gobbi, T. Nakamura, T. Tsuda, and S. Fukao (1999), Response of the Airglow OH Emission, Temperature and Mesopause Wind to the Atmospheric Wave Propagation over Shigaraki, Japan, *Earth Planets Space*, *51*, 863–875.

Taylor, M. J., M. B. Bishop, and V. Taylor (1995), All-sky measurements of short period waves imaged in the OI(557.7 nm), Na(589.2 nm) and near infrared OH and O(0,1) nightglow emissions during the ALOHA-93 campaign, *Geophys. Res. Lett.*, *22*, 2833–2836, doi:10.1029/95GL02946.

Tsugawa, T., A. Saito, Y. Otsuka, M. Nishioka, T. Maruyama, H. Kato, T. Nagatsuma, and K. T. Murata (2011), Ionospheric disturbances detected by GPS total electron content observation after the 2011 off the Pacific coast of Tohoku Earthquake, *Earth Planets Space*, *63*, 875–879.

Vadas, S. L. (2007), Horizontal and vertical propagation and dissipation of gravity waves in the thermosphere from lower atmospheric and thermospheric sources, *J. Geophys. Res.*, *112*, A06305, doi:10.1029/2006JA011845.

Vadas, S. L., and M. Nicolls (2009), Temporal evolution of neutral, thermospheric winds and plasma response using PFISR measurements of gravity waves, *J. Atmos. Sol. Terr. Phys.*, *71*, 740–770.

Yue, J., S. L. Vadas, C.-Y. She, T. Nakamura, S. Reising, H. Liu, P. Stamus, D. Krueger, W. Lyons, and T. Li (2009), Concentric gravity waves in the mesosphere generated by deep convective plumes in the lower atmosphere near Fort Collins, Colorado, *J. Geophys. Res.*, *114*, D06104, doi:10.1029/2008JD011244.

Yue, J., L. Hoffmann, and M. Joan Alexander (2013), Simultaneous observations of convective gravity waves from a ground-based airglow imager and the AIRS satellite experiment, *J. Geophys. Res. Atmos.*, *118*, 3178–3191, doi:10.1002/jgrd.50341.